JGR Space Physics

RESEARCH ARTICLE
10.1029/2024JA033169

Kinetic Alfven Waves Driving Auroral O+ Ion Outflows to Form Plasma Cloak During the 17 March 2015 Geomagnetic Storm

S. Tian[1], J. Li[1], C.-P. Wang[1], Q. Ma[1,2], J. Bortnik[1], C. P. Ferradas[3], J. Liu[4], Y. Shen[4], and L. R. Lyons[1]

[1]Department of Atmospheric and Oceanic Sciences, University of California, Los Angeles, CA, USA, [2]Center for Space Physics, Boston University, Boston, MA, USA, [3]Geospace Physics Laboratory, NASA Goddard Space Flight Center, Greenbelt, MD, USA, [4]Department of Earth, Planetary, and Space Sciences, University of California, Los Angeles, CA, USA

Key Points:

- Observations suggest that kinetic Alfven waves drive the O+ outflows from the nightside auroral region
- The auroral O+ outflows provide adequate flux for the newly formed plasma cloak
- Ion energization and auroral acceleration occur symmetrically in both hemispheres

Supporting Information:

Supporting Information may be found in the online version of this article.

Correspondence to:

S. Tian,
ts0110@atmos.ucla.edu

Citation:

Tian, S., Li, J., Wang, C.-P., Ma, Q., Bortnik, J., Ferradas, C. P., et al. (2025). Kinetic Alfven waves driving auroral O+ ion outflows to form plasma cloak during the 17 March 2015 geomagnetic storm. *Journal of Geophysical Research: Space Physics*, *130*, e2024JA033169. https://doi.org/10.1029/2024JA033169

Received 25 SEP 2024
Accepted 30 DEC 2024

Abstract We present multi-platform observations of plasma cloak, O+ outflows, kinetic Alfven waves (KAWs), and auroral oval for the geomagnetic storm on 17 March 2015. During the storm's main phase, we observed a generally symmetric equatorward motion of the auroral oval in both hemispheres, corresponding to the plasmasphere erosion and inward motion of the plasma sheet. Consequently, Van Allen Probes became immersed within the plasma sheet for extended hours and repeatedly observed correlated KAWs and O+ outflows. The KAWs contain adequate energy flux toward the ionosphere to energize the observed outflow ions. Adiabatic particle tracing suggests that the O+ outflows are directly from the nightside auroral oval and that the energization is through a quasi-static potential drop. The O+ outflows from the nightside auroral oval were adequate (10^8-10^9 #/cm^2-s) and prompt (several minutes) to explain the newly formed plasma cloak, suggesting that they were a dominant initial source of plasma cloak during this storm.

Plain Language Summary The plasma cloak is a plasma population located around the geospace where the magnetic field transits from Earth dominated to solar wind affected. Traditionally, scientists suggest that low energy ions that flow out from the Earth's polar region are what eventually form the plasma cloak. Recently, nightside observations suggest that high energy ions that flow away from the nightside ionosphere may provide another important contribution. Although it is well known that the former's number flux is much larger, we show the latter alone is adequate and prompt enough to explain the newly formed plasma cloak during the geomagnetic storm on 17 March 2015. Dayside ions may still be important in sustaining the newly formed plasma cloak but nightside ions are suggested to be the dominant source for the initial formation. In addition, our observations suggest that the nightside ion outflows are driven by the Alfven wave (a common low-frequency wave in magnetized plasma).

1. Introduction

The plasma cloak, or warm plasma cloak, is a bi-directional plasma population outside the plasmapause (Chappell et al., 2008). The typical energy range of plasma cloak ions is 10–100s eV. Chappell et al. (2008) suggest that the low-energy ionospheric ion outflows (1–10s eV) can be accelerated to 10–100s eV by the centrifugal force as they travel along the open field lines that thread the polar cap (Cladis, 1986; Horwitz et al., 1994). Following the global-scale convection, these ions enter the distant plasma sheet and convect toward the Earth (Stern, 1975; Volland, 1973). They eventually accumulate outside the plasmapause, flow along the Alfven layers, and form the plasma cloak. In this scenario, the entire ion circulation from the ionosphere to the plasmapause lasts several hours according to a numerical simulation (Chappell et al., 2008).

Recent observations show that the nightside auroral oval could provide a more immediate and "energy-ready" source for the plasma cloak. In contrast to the 1–10 eV source ions suggested by Chappell et al. (2008), the auroral ion outflows are already energized to 10–100s eV. The new mechanism of forming plasma cloaks from these high energy ions is suggested by recent observations in the inner magnetosphere (within 6 R_E) (Nosé et al., 2022) and the plasma sheet (~8 R_E) (Wang et al., 2023). Outflows of <1 keV ions from the ionosphere have been frequently observed several minutes after individual dipolarizations (Gkioulidou et al., 2019; Nosé et al., 2016). The energy-time dispersion of these ions can be reproduced by launching test particles from the nightside auroral region

(Gkioulidou et al., 2019; Nosé et al., 2022). These ions will also follow the Alfven layer, dwell outside the plasmapause, and contribute to the plasma cloak (Nosé et al., 2022). It has been well known that the ion outflows within the Earth's magnetosphere are primarily from the high-latitude ionosphere, including the cusp (or the dayside auroral region), polar cap, and nightside auroral region (André & Yau, 1997; Moore, Lundin, et al., 1999; Yau & André, 1997). The relative contribution of outflows from these regions to the plasma cloak needs to be evaluated.

Another key question is how the ion outflows that form the plasma cloak are energized. At low altitudes (e.g., below 2 R_E altitude), ion conics and beams are often observed, suggesting two general types of energization mechanisms, that is, perpendicular heating and parallel acceleration, respectively (André & Yau, 1997; Moore, Lundin, et al., 1999; Yau & André, 1997). The polar cap ion outflows could experience centrifugal acceleration (Cladis, 1986; Horwitz et al., 1994). The nightside auroral ion outflows could be accelerated by the quasi-static field-aligned potential drop or heated perpendicularly by various waves (Paschmann et al., 2003). The latter is mass dependent whereas the former is not, therefore we will analyze the energy-time dispersion for both the H+ and O+ ions to discuss the energization mechanisms.

2. Instrumentation

The key observations used in this study include the auroral observations from the ground-based all-sky imager (ASI) of the THEMIS mission (Mende et al., 2008) and SSUSI instrument onboard the DMSP spacecraft (Paxton et al., 2002), the low-altitude (~800 km altitude) observations on ion velocity (the SSJ instrument) from DMSP (Hardy, 1984), and the high-altitude observations on the thermal plasma (Funsten et al., 2013) and electric (Breneman et al., 2022; Wygant et al., 2013) and magnetic (Kletzing et al., 2013) waves in the inner magnetosphere from the Van Allen Probes (RBSP-A and -B).

The DC electric and magnetic fields are used to calculate the Poynting flux. The latter is in 3D whereas the former is in the 2D spin plane. The spin axis E field is calculated using the $\vec{E}\cdot\vec{B}=0$ assumption. This assumption is good for magnetohydrodynamic (MHD) plasmas. It also works for KAWs, because the KAWs' parallel E field is finite but usually much smaller than the perpendicular E field. The Poynting flux is calculated in the time-frequency domain and integrated over frequency. For a certain frequency in the spacecraft's frame f_{SC}, the Poynting flux is $\vec{S}_{f_{SC}}(t)=\alpha\vec{E}_{f_{SC}}(t)\times\vec{B}_{f_{SC}}(t)$, where α is a constant that scales the unit of the Poynting flux to mW/m^2 for the electric field in mV/m and magnetic field in nT, and the electric and magnetic field at f_{SC} are obtained by the Morlet wavelet transform.

3. Observations

The 17 March 2015 geomagnetic storm features strong magnetopause erosion down to 6.6 R_E (Le et al., 2016). Coincidental with the strong erosion, the plasmapause shrunk to L<3 (Figure 1) presumably due to strong convection, and the nightside auroral oval extended equatorward to magnetic latitude (MLat) <50 deg in both hemispheres approximately symmetrically (Figure 2). Under such conditions, the Van Allen Probes were well within the plasma sheet and were in prolonged magnetic conjunction with the auroral oval. This allows the twin probes to continuously monitor the ion outflows and wave activities within the plasma sheet, and to survey different plasma regions including the inner boundary of the plasma sheet, the plasma cloak, and the plasmapause multiple times.

3.1. Erosion of Plasmasphere

Figure 1 shows the temporal evolution of the plasmapause location during the 17 March 2015 geomagnetic storm. Plasmapause is defined as the location where the spacecraft passes the 100 cm^{-3} plasma density, following previous literature using RBSP data (Ripoll et al., 2022; Thaller et al., 2019). For multiple passes per orbit, we use the averaged location (e.g. 09:49 UT for RBSP-A, Panel c). Panels (a and b) show where and when the plasmapause was located. They are color-coded by time, where a darker color indicates a later time. The plasmapause decreased to lower L values during the storm's main phase and recovered afterward (Panel b). The deepest erosion occurred around the end of the main phase, reaching L~2.5 (Panel a). In the next section, we show that the temporal evolution of the plasmapause during the main phase was consistent with the equatorward motion of the auroral oval in both hemispheres.

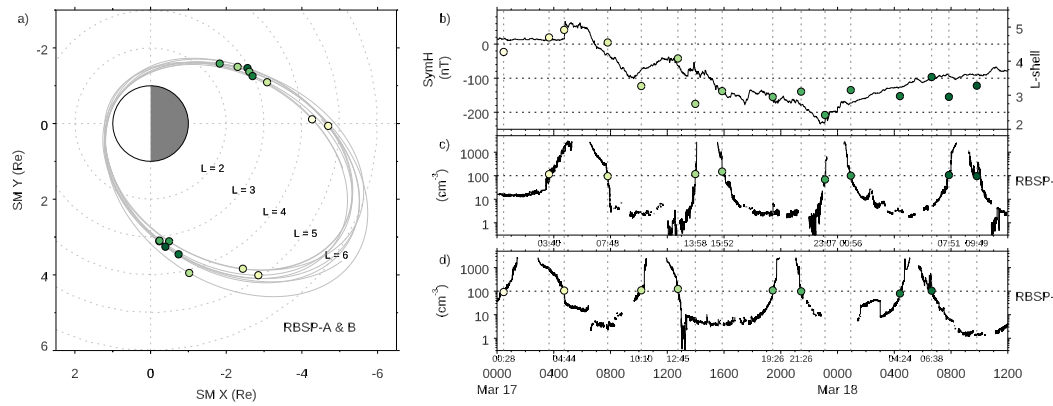

Figure 1. The temporal evolution of the plasmapause location during the geomagnetic storm on 17 March 2015. Panel (a) shows the orbits of RBSP-A and -B in the equatorial plane. The colored circles mark the location of the plasmapause, defined as the average location of 100 cm^{-3} plasma density. Darker colors indicate later times. Panels (c and d) show the plasma density derived from the upper hybrid line for RBSP-A and B, respectively. Panel (b) shows the SymH index during the storm and the determined plasmapause locations. During the storm main phase, the plasmapause location decreased from L∼4.5 to L ∼2.5-3.

3.2. Symmetric Equatorward Motion of the Auroral Oval

Figure 2 shows auroral snapshots from DMSP during the storm's main phase. The snapshots are selected to form two groups, one around the beginning of and another around the end of the main phase. The auroral images in both groups show a clear equatorward motion of the auroral oval, coinciding with the decrease of the Sym-H index (Panel a). Conjugate observations from the ASI in the northern hemisphere were available at the beginning of the main phase. The ASI auroral movie in the Movie S1 shows a spatial and temporal evolution of the auroral oval that is similar to the DMSP snapshots but with much more details. As a simple comparison, Figure 2 shows 4 snapshots (Panels c-1 to c-4) from Movie S1 around the time of the DMSP snapshots (Panels b-1 to b-4). Symmetric equatorward motion of auroral features can be identified, including the initial auroral oval at high latitude (∼65 deg MLat, Panels b-1 and c-1), the post-midnight bulge as an onset of auroral substorm (Panels b-2 and c-2), the stronger auroral emission in post-midnight (Panels b-3 and c-3), and the omega bands in post-midnight and stronger auroral emission in pre-midnight (Panels b-4 and c-4). Although not identical, these features are generally symmetric in both hemispheres.

To quantitatively link to the plasmapause location shown in Section 3.1, we assume a dipole field $1/L = \cos^2 \lambda$, where λ is the magnetic latitude. Figure 1 shows that the plasmapause was around L∼2.5 at the end of the storm's main phase (Figure 1a), which is very close to the Earth. This L value corresponds to the magnetic latitude of $\lambda = 50$ deg. Note that beyond 3 Re, the dipole assumption is invalid as the observed magnetic field was highly stretched (Figures 3a and 4a). However, the dipole assumption is probably valid for $|R| < 3$ Re as the observed magnetic field's tilt angle became consistent with the model (e.g., Figure 3a after 10:00 UT and Figure 4a after 13:50 UT). In Figure 2, Panel (b-8) was taken around the end of the main phase. It shows that the equatorward boundary reached around 50 deg. Therefore, the plasmapause is quantitatively consistent with the equatorward boundary of the auroral oval. The erosion of the plasmapause is consistent with the equatorward motion of the auroral ovals in both hemispheres.

3.3. Correlated KAWs and O+ Outflows Within the Plasma Sheet

As shown in the previous sections, a general correlation existed between the auroral oval's equatorward motion and the plasmasphere's erosion during the storm's main phase. Figure 3 shows the point observation from RBSP-B around 06:30 UT, when the spacecraft experienced the stretching of the plasma sheet magnetic field. In addition, the Movie S1 shows a clear equatorward motion of the auroral oval from 06:15 UT to 06:45 UT. This is the classic signature of the substorm growth phase. It corresponds to the inward motion of the plasma sheet and the local magnetic fields become more stretched and map to lower latitudes in the ionosphere (Yue et al., 2015). The local stretching is evidenced by the sharp decrease of the tilt angle of the RBSP-B's local magnetic field (Figure 3a, shaded region). After 08:50 UT, RBSP-B observed a gradual increase in the magnetic tilt angle. This change is

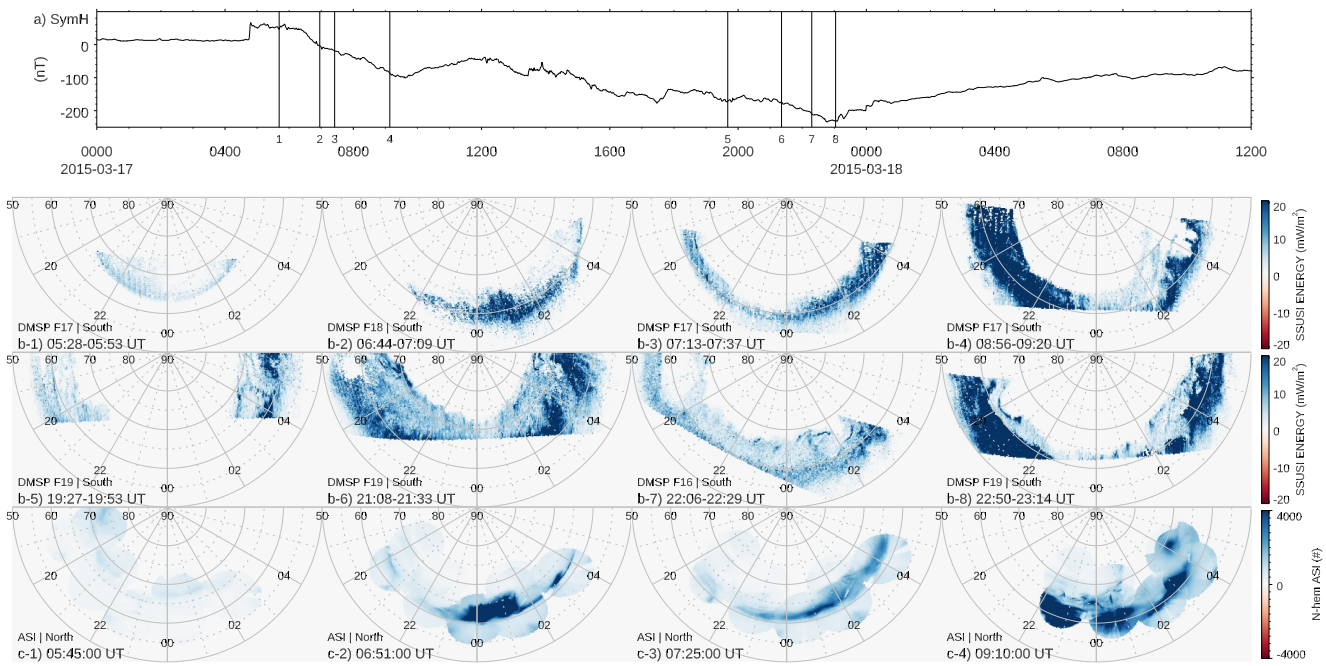

Figure 2. Snapshots of the aurora in the southern and northern hemispheres during the main phase of the 17 March 2015 storm. Panel (a) shows the Sym-H index. Panels (b-1 to b-4) and Panels (b-5 to b-8) show two groups of auroral activities from DMSP observations, around the beginning and end of the main phase respectively. The corresponding times are indicated in Panel (a). Regardless of the MLT dependence, the equatorward boundary of the auroral oval around 21 MLT moved from around 65 deg (Panel b-1) to 50 deg (Panel b-8). Panels (c-1 to c-4) present the corresponding northern hemisphere ASI snapshots of those in Panels (b-1 to b-4), showing a generally symmetric temporal and spatial evolution.

probably due to the spacecraft's motion because the auroral oval did not move significantly in the northern and southern hemispheres (Movie S1). As RBSP-B moved toward its perigee, it sampled the radial profile of the stretching, which diminished around L∼3.5 (10 UT, Panels a and k).

We infer that RBSP-B was in the plasma sheet from 04:44 UT to 10:10 UT, based on the plasmapause locations (Figure 1d), because the plasmapause is the Alfven layer for cold electrons and is usually a good inner boundary for the electron plasma sheet. This is also consistent with the existence of >1 keV electrons and H+ ions (Figures 3c and 3d). Several groups of strong broadband waves were observed within the plasma sheet, marked by the vertical red lines in Figures 3g and 3h for the magnetic and electric fields, respectively. Figures 3e and 3f show that these waves correlate well with energy-time dispersed O+ ions. This correlation is consistent with previous reports (Hull et al., 2019; Liu & Zong, 2022). RBSP-A observed the same correlation, which was essentially behind RBSP-B by 4 hr (Figure 4).

These broadband waves are routinely observed in the plasma sheet. They do not have frequency peaks around the ion cyclotron frequencies and thus are not ion cyclotron waves. Chaston et al. (2015) have shown that these waves are kinetic Alfven waves (KAWs). In the following, we explicitly verified that they are KAWs using commonly used criteria in the literature (e.g., Chaston et al., 2015; Tian et al., 2022). The results are shown in Figure 5. For the 4 wave packets marked by the red bars (Panel b), we examined the E/B ratio using the measured electric and magnetic fields (black curves in Panels (c-1 to c-4). Note that because the electric field data contain artificial power around the spacecraft's spin frequency, the E/B ratio around this frequency is removed. The measured E/B ratio is compared with the dispersion relation of KAWs (Lysak & Lotko, 1996)

$$\frac{\omega}{k_{\|}} = v_A\sqrt{1+k_{\perp}^2\rho_i^2}, \tag{1}$$

where ω and $k_{\|}$ are the angular frequency and parallel wave vector in the plasma's rest frame, $v_A = B_0/\sqrt{\mu_0 n m_i}$ is the local Alfven speed, $\rho_i = \sqrt{k_B T_e/m_i}/\omega_{ci}$ is the ion acoustic gyro-radius related to the electron temperature T_e, ion mass m_i, and ion cyclotron angular frequency ω_{ci}. In the spacecraft's frame, the dispersion relation can be approximated, in the plasma sheet, by (e.g., Chaston et al., 2015)

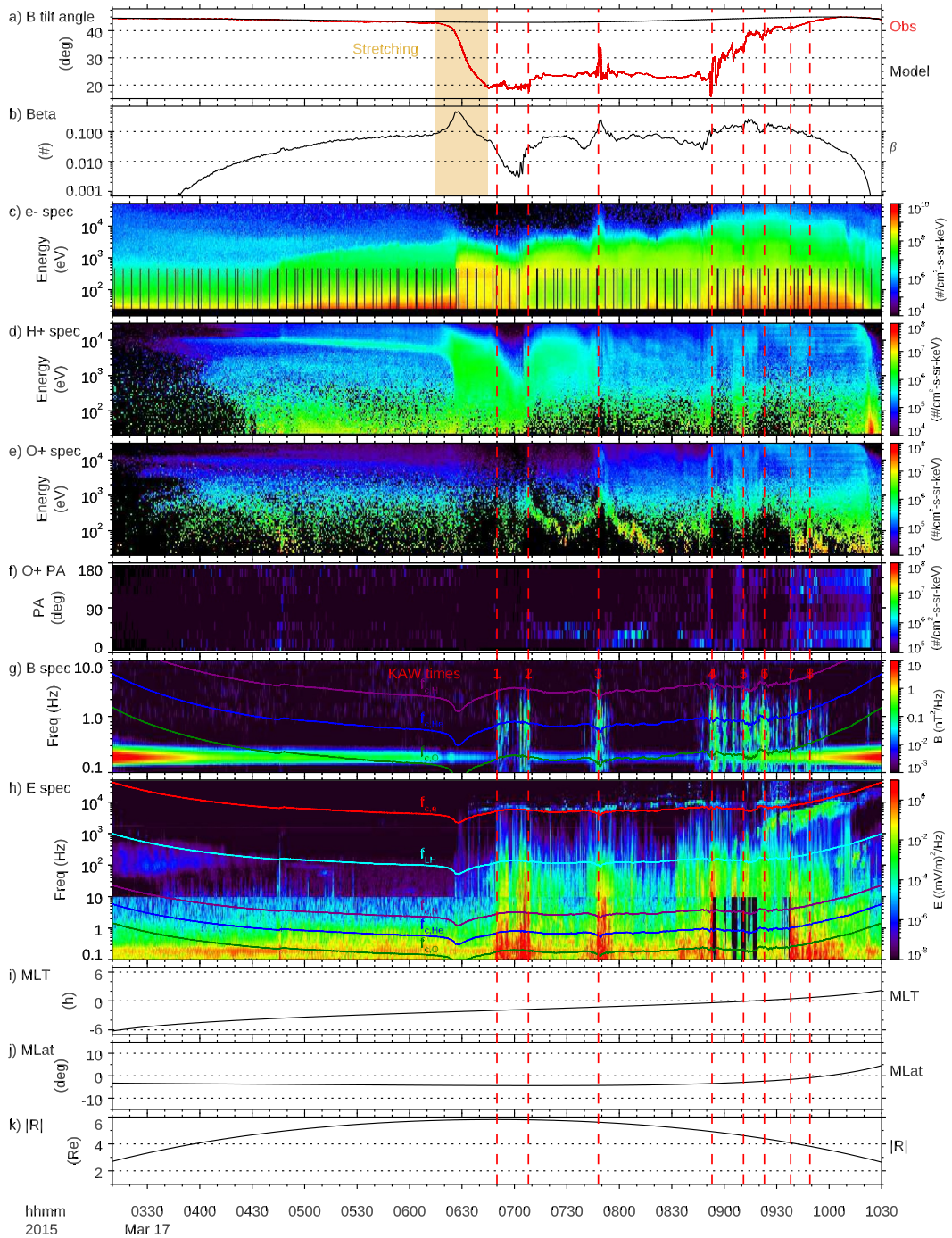

Figure 3. RBSP-B observations on KAWs and O+ outflows during the plasma sheet thinning. Panel (a) shows the tilt angle of the observed (red) and model (black, T89) magnetic field. Here the tilt angle is defined as $\arcsin(B_z/|B|)$. Panel (b) shows the plasma beta. Panels (c to e) show the omnidirectional energy spectrograms for the electron, H+, and O+ ions respectively. Panel (f) shows the pitch angle spectrogram for O+ ions above 50 eV. Panels (g and h) show the wave magnetic and electric field activities. Vertical red lines mark the times of KAWs seen in these two panels. The lines mark the cyclotron frequencies for electron (red), H+ (purple), He+ (blue), O+ (green), and the lower hybrid frequency (cyan). Panels (i to k) show the spacecraft position, including the MLT, MLat, and $|R|$.

$$\frac{E_{\perp,out}}{B_{\perp,west}} \simeq v_A \sqrt{1+\frac{f_{SC}^2 \rho_i^2}{v_f^2}}, \tag{2}$$

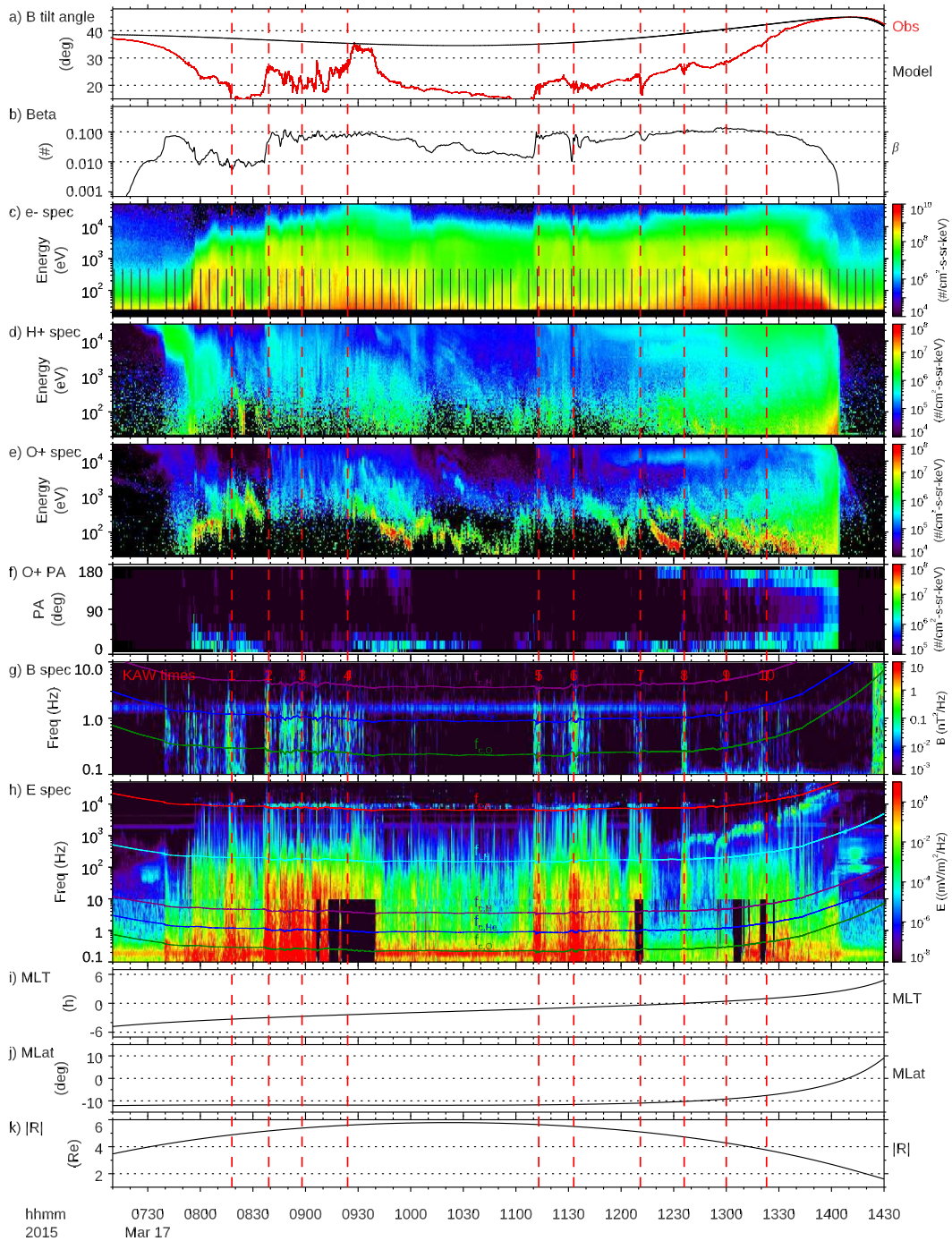

Figure 4. RBSP-A observations on KAWs and O+ outflows after the plasma sheet thinning. The panels are in the same format as Figure 3.

where f_{SC} is the wave frequency in the spacecraft's frame, v_f is the plasma's flow speed. Here, we used a typical flow speed $v_f = 50$ km/s. The ion mass is the average of H+ and O+ ions $m_i = (n_H m_H + n_O m_O)$. The H+ and O+ densities n_H and n_O are determined from the HOPE measurements. Figure 5 shows that the measured E/B ratio for the 4 selected wave packets is comparable to the KAWs' dispersion relation over the covered frequency range. The local plasma beta (β) is in the range of $\beta \in [m_e/m_i, 1]$ (Figure 3b), which is consistent with the plasma beta range corresponding to the kinetic Alfven waves (inertial Alfven waves have $\beta \ll m_e/m_i$) (Lysak, 2023; Lysak & Lotko, 1996).

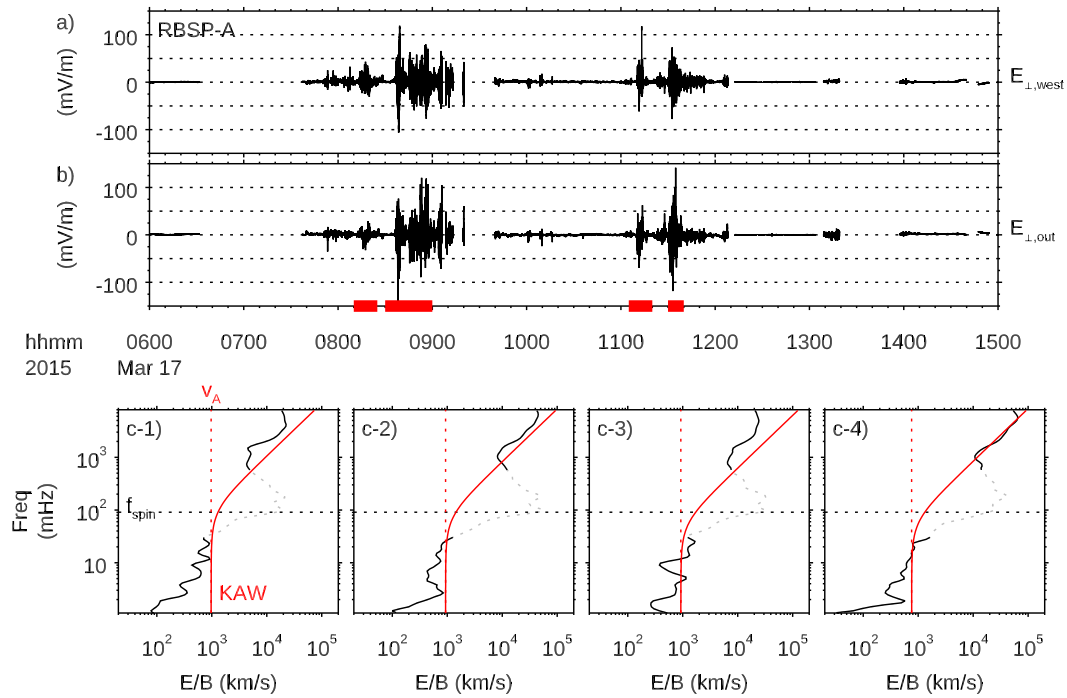

Figure 5. The electric fields and E/B ratio of KAWs. Panels (a and b) show the electric fields in the two perpendicular directions. Panels (c-1 to c-4) show the E/B ratio as a function of the frequency in the spacecraft frame during four sectors of strong KAWs. The E fields contain a strong spin tone (cf. Figure 4h), causing an artificial local peak around the spin frequency (~100–200 mHz) in the E/B ratios. The red curves mark the expected dispersion for KAWs.

We note that for KAWs, the wave frequency in the plasma's rest frame should be much smaller than the ion cyclotron frequencies ($f_{c,H}$ and $f_{c,O}$). However, considering the Doppler shift $f_{SC} = f + \vec{k}\cdot\vec{v}_f/2\pi \simeq f + k_\perp v_{f,\perp}$, where we used that KAWs have $k_\perp \gg k_\parallel$. Thus, KAWs at large $k_\perp$ appear as high frequency waves in the spacecraft's frame (e.g. Panel (h) in Figures 3 and 4). Another point to note is that KAWs at high frequency (AC E field) are often better observed than KAWs at low frequency (DC E field). For example, in Panel h) in Figures 3 and 4, there are data gaps in the DC E field below 10 Hz, whereas the AC data are continuous in time and better show the distribution of KAWs.

3.4. Tracing O+ Outflows to Nightside Auroral Oval

Energy-time dispersed O+ outflows have been reported extensively in the nightside plasma sheet (e.g., Gkioulidou et al., 2019; Hull et al., 2019; Keiling et al., 2004, 2006; Nosé et al., 2016). As shown in this and previous studies, the highest energy O+ outflows are typically 1–10 keV and appear several minutes after strong Alfven waves and/or dipolarizations are observed in the plasma sheet. They are then followed by an energy-time dispersion tail down to about 10 eV that lasts several 10s min. Given that the time of flight for keV O+ over several R_E along the magnetic field is about several minutes, the short time delay suggests that these O+ probably originate from the nightside ionosphere. Here we use the energy-time dispersion observed in multiple ion species (H+ and O+) to demonstrate that these outflows are directly from the ionosphere within the nightside auroral oval.

Figure 6 shows a simple test particle simulation. The RBSP-A data within this time range are used because both H+ and O+ ions showed clear energy-time dispersions. We use the energy-time dispersion of O+ in the parallel direction and the measured pitch angle (~15 deg, Panel c) as inputs (magenta dots in Panel a) to trace their adiabatic motion backward in time and altitude. We located that the O+ are energized around 1.2 R_E altitude around 12:34-12:38 UT and along the field lines threading the nightside auroral oval. The solved initial time and altitude are listed in Panel (a). With these initial conditions, we launch the test particles (H+ and O+ ions) from both hemispheres and let them bounce adiabatically. Here, we adopted the time-stationary T89 model (Tsyganenko, 1989), but other Tsyganenko models (T96, T01, T04s) produce essentially the same results (not shown). The simulated energy-time dispersion (red and orange dots for the first and second appearances respectively) agrees reasonably well with

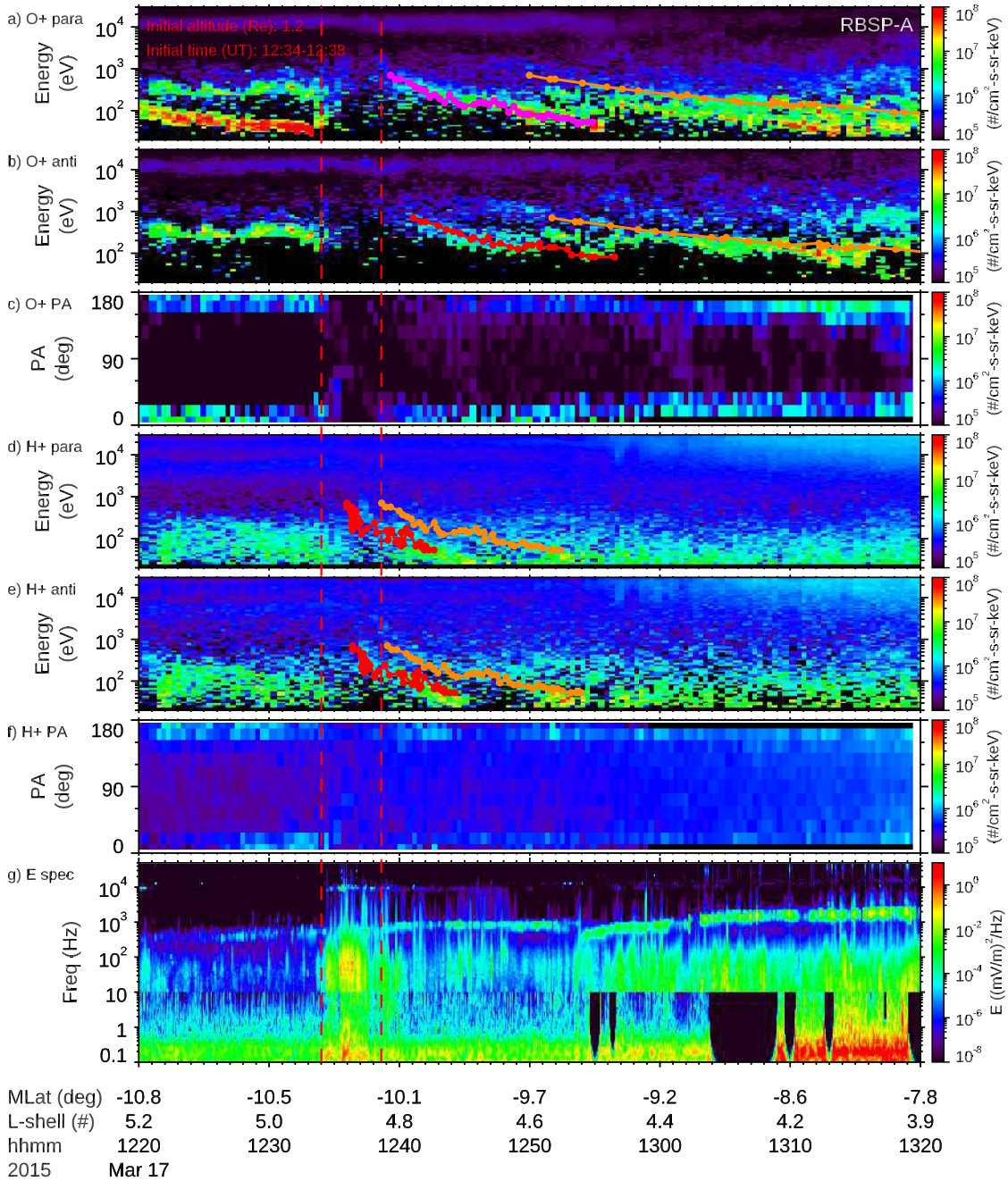

Figure 6. The energy-time dispersed ions (O+ and H+) from RBSP-A measurements, which is around the #8 KAW times in Figure 4. Panels (a and b) show the O+ energy spectrogram along the parallel and anti-parallel directions respectively. Note that the spacecraft was in the southern hemisphere. Panel (c) shows the O+ pitch angle distribution. Panels (d to f) are in the same format for H+. Panel (g) shows the wave electric field power spectrogram. The magenta dots in Panel (a) mark the selected test particles' time and energy. They are used to derive the initial conditions for our particle tracing. The red and orange dots are the simulated results for the first and second appearances, respectively.

observations (Panels b, d, and e), suggesting that the ion outflows are directly from the nightside auroral oval, rather than from the cusp or polar cap, and that the ion outflows are in general symmetric in both hemispheres.

3.5. KAWs Energize O+ Outflows (and Discrete Auroral Emission)

Interestingly, the time of the expected initial energization (12:34 UT to 12:38 UT) coincides well with the time of intense KAWs (Figure 6f). Considering the travel time for KAWs to the ionosphere is about 10 s for RBSP-A, our

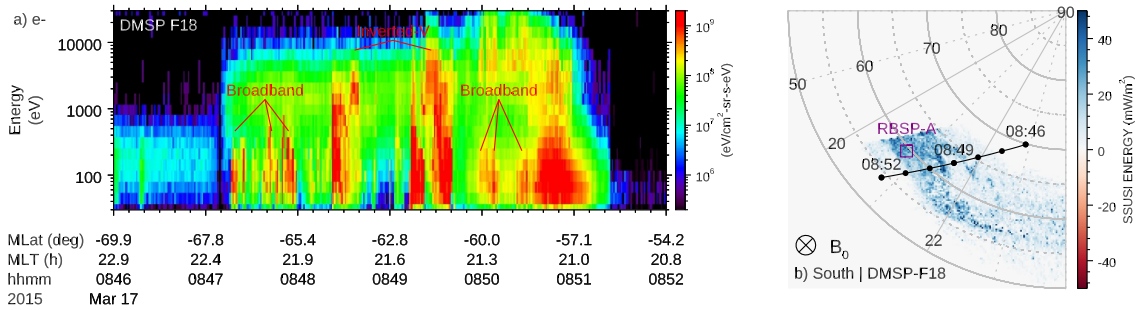

Figure 7. The DMSP F18 crossing over the auroral oval in the southern hemisphere. Panel (a) shows the electron energy spectrogram. Inverted-V and broadband electrons were observed, indicating acceleration from a quasi-static potential drop and dispersive Alfven waves within the auroral acceleration region. (b) The DMSP pass and the auroral oval. The auroral oval's energy flux was about 26 mW/m^2. The footpoint of RBSP-A was close to the track of DMSP F18. Although the uncertainty of the footpoint's MLat could be large, RBSP-A was in conjunction with the auroral oval, as indicated from the O+ outflows in Section 3.4.

observation and simulation show clear evidence for the correlation between KAWs and O+. Figure 8 further evaluates the energy budget within the magnetosphere-ionosphere (M-I) system. Panel (c) in Figure 8 compares the energy fluxes of the KAWs ($S_{\text{Earthward}}$, Poynting flux toward the Earth, blue) and that of the O+ outflows ($\Gamma_{\text{O,outward}}$, O+ kinetic energy flux away from the Earth, green). The latter is computed from the test particles marked by magenta dots in Panel a) in Figure 8. This orbit is chosen because the Poynting flux calculation can be reliably performed over most of the orbit. However, frequent data gaps still exist because of the lack of valid electric field measurements (Panel c). For example, there was an ion dispersion that started around 09:30 UT. However, the Poynting flux is missing due to data gaps and thus cannot be directly compared to the ion kinetic energy flux around this time.

Regardless of the data gap, for the times when both $S_{\text{Earthward}}$ and $\Gamma_{\text{O,outward}}$ are available, we observed that the former is usually much larger, especially at the beginning of individual O+ dispersions. For example, there were several outflow dispersions from 08 UT to 08:40 UT. They have $\Gamma_{\text{O,outward}}$ peaks at 1–10 mW/m^2. The $S_{\text{Earthward}}$ peaks were about 10 mW/m^2. However, we note that the ion energies are "spread out" because of the time of flight effect that causes the dispersion. Therefore, comparing the integrated values over time may be better than the instantaneous values. Because of the frequent data gap, we just perform a very rough estimation over the entire orbit. The typical value of $S_{\text{Earthward}}$ peaks is 10–100 mW/m^2, whereas that of $\Gamma_{\text{O,outward}}$ is 1–10 mW/m^2. Therefore, we estimate that $\Gamma_{\text{O,outward}}$ is about 10% of $S_{\text{Earthward}}$, that is, 10% the energy of KAWs is converted to the kinetic energy of the O+ outflows. The energy budget demonstrates that KAWs are sufficiently intense to energize the O+ outflows.

During this orbit, there was one conjunction around 08:51 UT between RBSP-A and DMSP F18 during which we can obtain the energy flux of the auroral emission. DMSP F18 crossed the auroral oval (Figure 7b) and was slightly eastward of RBSP-A's footprint, observing both inverted-V and broadband electrons (Figure 7a). Here, the uncertainty of the MLat of the RBSP-A footpoint could be large, because of the significant stretching of the magnetic field in the plasma sheet (Figure 4a). However, as indicated from the O+ outflow tracing in Section 3.4, RBSP-A was probably in conjunction with the auroral oval. The broadband electrons seen by DMSP F18 are a classical signature of Alfvenic acceleration. This is consistent with the strong KAWs seen by RBSP (Figure 5), providing further evidence that RBSP-A was in conjunction with the auroral oval.

Around the time of this conjunction, the Poynting flux of the KAWs was about 70 mW/m^2 (Figure 8c), the energy flux of the auroral emission was 26 mW/m^2 (Figures 7b and 8c red dot), and the kinetic energy flux of the O+ outflow was much smaller because the dispersion was weak. However, the comparison provides a rough estimate of the energy partition: the auroral emission is a more significant fraction (37%) of the energy flux of the KAWs than O+ (10%). Overall, KAWs are capable of energizing both the O+ outflows and the auroral emission. Note that we cannot reliably estimate $\Gamma_{\text{H,outward}}$ because it is difficult to distinguish the H+ ions from the ionosphere from those within the plasma sheet. However, if we assume that $\Gamma_{\text{H,outward}}$ is comparable to $\Gamma_{\text{O,outward}}$, the kinetic energy flux of the ion outflows would increase to about 20% of the energy flux of the KAWs.

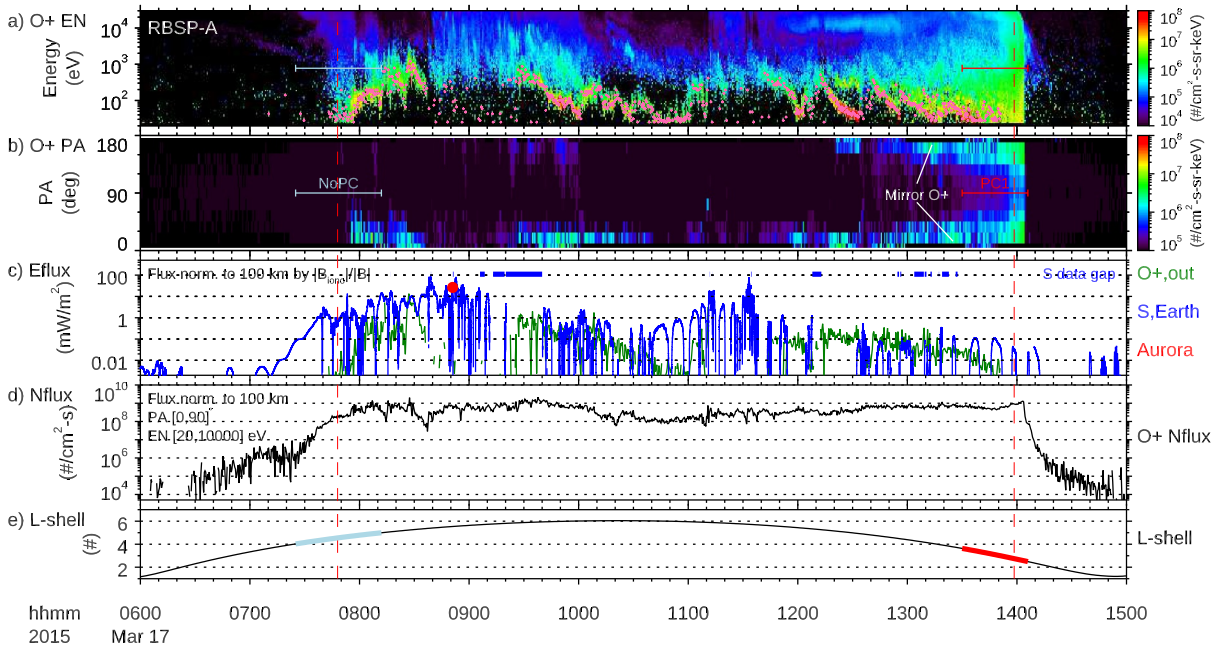

Figure 8. Energy flux and number flux of O+ outflows before forming plasma cloak. Panels (a and b) show the O+ energy and pitch angle spectrograms in the same format as in Panels (e–f) in Figure 4. The pitch angle spectrogram is for 20 eV to 30 keV. Panel (c) shows the integrated kinetic energy flux for the O+ outflows (green), the Earthward Poynting flux due to KAWs (blue), and the energy flux of the auroral emission (red). Data gaps in Poynting flux are marked by the blue bars. The O+ kinetic energy flux is calculated from the magenta points in Panel (a). They correspond to the peak flux for each time. Panel (d) shows the integrated parallel number flux of the O+ outflows over the pitch angle of [0,90] deg and energy of [20 eV, 10 keV]. Panel e shows the L-shell of RBSP-A. The observations show that the Poynting flux due to KAWs is adequate to power the O+ outflows and that the number flux of the O+ outflows is comparable to the formed plasma cloak. PC and NoPC stand for plasma cloak and no plasma cloak respectively. The plasma cloak is when both parallel and anti-parallel O+ ions are observed (not the mirroring or outflowing O+ ions).

3.6. O+ Outflows as the Dominant Source for a Newly Formed Plasma Cloak

Figure 8 shows the appearance of a newly formed plasma cloak, which is characterized by the high flux (>10^5 #/cm^2-s-sr-keV) in 100s eV (Panels a) and around both 0 and 180 deg pitch angles (Panel b). More orbits for both RBSP-A and -B are shown in Figure 9. The first appearance of the plasma cloak was around 14:00 UT at RBSP-A (Figure 8) and around 10:00 UT at RBSP-B (Figure 9). Note that before the first appearance, no plasma cloak was observed when the spacecraft crossed the plasmapause (light blue, red vertical line for plasmapause). In contrast, later orbits saw plasma cloaks around the plasmapause twice per orbit (Figure 9). Therefore RBSP-A (and -B) observed the emergence of a newly formed plasma cloak.

Figure 8 shows that significant O+ outflows (Panels a and b) were observed within the orbit when the plasma cloak emerged. These O+ outflows directly originated from the nightside auroral oval (Section 3.4), rather than from the dayside cusp or polar cap. Panel (d) shows that the number flux of the O+ outflows is consistent with that of the newly formed plasma cloak. For example, the plasma cloak around 14 UT has a number flux of about 10^9 #/cm^2-s. The mirroring O+ outflows' number flux was around $5 \times 10^8 - 10^9$ #/cm^2-s. The peak number flux during this orbit was 2×10^9 #/cm^2-s, observed around the ion outflows around 09:30 UT. Considering that all these O+ ions are likely to dwell outside the plasmapause, following the Alfven layer, the O+ outflows from the nightside auroral oval are an adequate and likely the dominant source for the newly formed plasma cloak.

4. Discussion

Based on the observations presented in Section 3 and unifying previous studies (Hull et al., 2019; Nosé et al., 2022), we propose the following physical mechanism for the newly formed plasma cloak (Figure 10): (a) KAWs are generated within the plasma sheet, and they propagate toward the ionosphere; (b) KAWs power the nightside emission of discrete auroras and energize O+ outflows directly from the nightside auroral oval; (c) these O+ outflows follow the convectional electric field and drift around the plasmapause, serving as the dominant

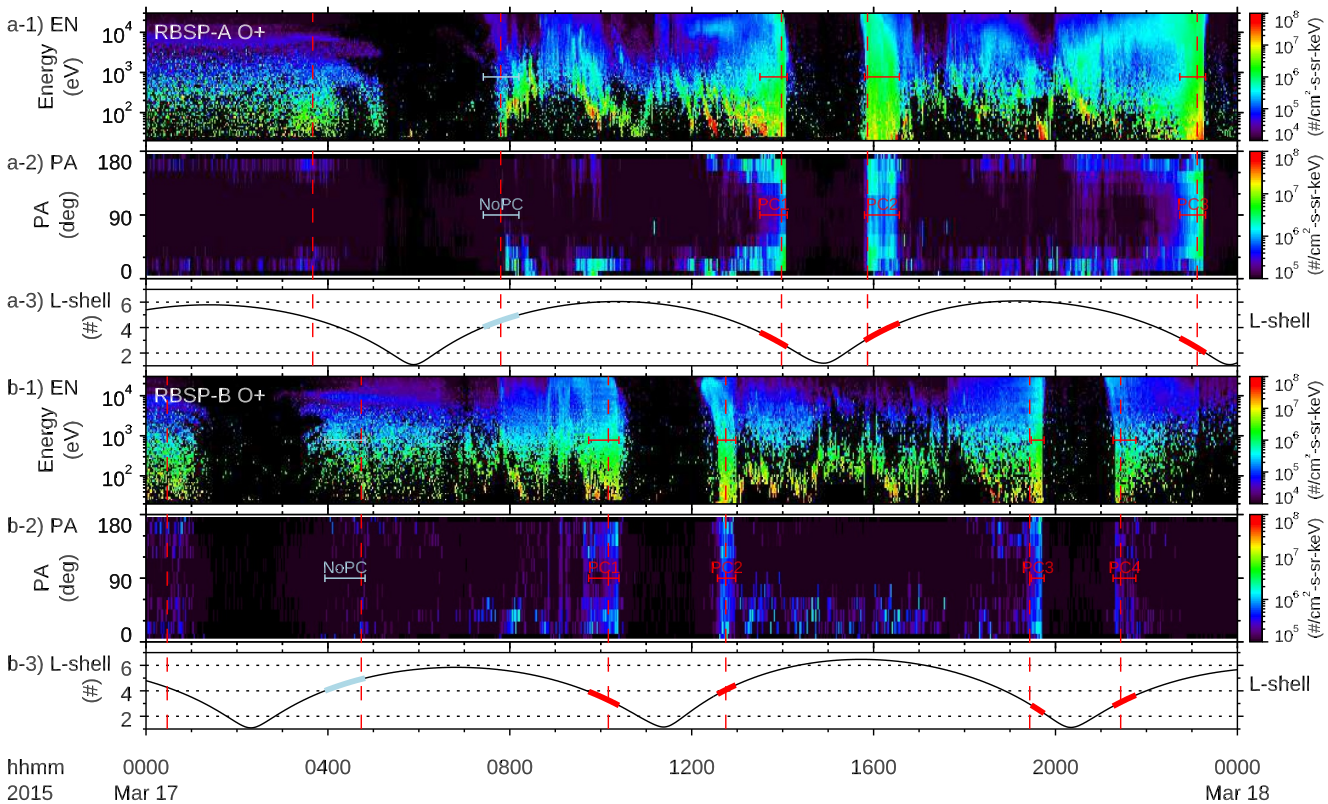

Figure 9. The appearance of the plasma cloak during the 17 March 2015 storm's main phase. Panels (a-1 to a-3) show the RBSP-A observations on the O+ energy spectrogram, pitch angle spectrogram, and L-shell. Panels (b-1 to b-3) show the RBSP-B observations in the same format. Plasma cloaks (PC) are marked by red in these panels. In addition, the orbit before the first appearance of the plasma cloak is marked by light blue.

source for the newly formed plasma cloak. The entire process could form a plasma cloak several minutes after the KAWs generation. The KAWs, ion outflows, and auroral emissions are generally symmetric around the magnetic equator.

The term KAW in this paper refers to the shear Alfven wave in a plasma where $m_e/m_i \ll \beta \ll 1$. KAWs have been routinely observed within the Earth's plasma sheet above 4 R_E altitude, where the above beta range is satisfied (Chaston et al., 2015; Tian et al., 2022; Wygant et al., 2002). KAWs within the plasma sheet are usually broadband in the spacecraft frame due to the Doppler shift, where high (low) frequency corresponds to small (large) wavelength. The wave power usually follows Kolmogorov's law (Chaston et al., 2015; Kolmogorov, 1941; Tian et al., 2021), suggesting a turbulent cascade from a much larger wavelength (MHD regime) to a much smaller wavelength (kinetic regime) than the scale of ion-acoustic gyroradius.

As in Kolmogorov's law (Kolmogorov, 1941), wave power is large at low frequency (MHD regime). Therefore, the total Poynting flux of KAWs is mostly due to the MHD Alfven waves. They propagate along the magnetic field, transmitting the power of KAWs to the auroral acceleration region (AAR) (Keiling et al., 2003; Wygant et al., 2000). Two acceleration mechanisms, including the quasi-static potential drop and Alfvenic acceleration, can occur within AAR, causing discrete auroral emissions in the ionosphere (Paschmann et al., 2003). During the propagation, a small portion of the wave power cascades to kinetic scales causing Alfvenic acceleration *en route*. However, most of the power of KAWs will be dissipated within AAR but not around the magnetic equator or before reaching AAR.

During the conjunction between RBSP-A and DMSP F18 around 08:50 UT, the latter observed the accelerated electrons from both acceleration mechanisms. Based on the comparisons between the Poynting flux of KAWs at RBSP-A and the energy flux of the discrete auroral emission (Figure 8c), we conclude that KAWs power the auroral emission. The efficiency is estimated to be 37%. Note that within and below AAR, $\beta \ll m_e/m_i$ and thus the kinetic Alfven wave becomes the inertial Alfven wave (IAW) (Lysak, 2023; Lysak & Lotko, 1996). However,

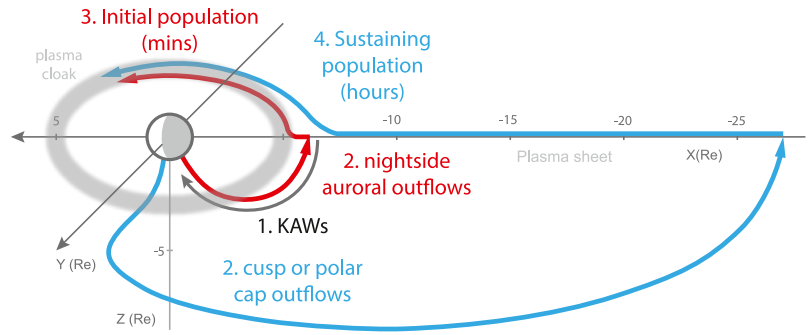

Figure 10. A schematic to summarize the processes in forming the plasma cloak. The guiding center motions of ion outflows (H+ and O+) are drawn with gyro and bounce motions omitted for the nightside auroral region (red) and cusp or polar cap (blue). KAWs drive ionospheric outflows from the nightside auroral oval. These auroral outflows convect Earthward and drape around the plasmapause due to the convectional electric field (Stern, 1975; Volland, 1973), providing the initial population in forming the plasma cloak in several minutes. Outflows from the cusp or polar cap go through a much more deviated path, providing the sustaining population for the plasma cloak in longer timescales. These processes should be generally symmetric around the magnetic equator but only the southern part is drawn for simplicity.

since the IAW is converted from KAW during its propagation, it is proper to state that KAWs power the discrete auroral emission.

The intense O+ outflows show a clear origin from the ionosphere. The question is whether the O+ outflows are directly from the nightside auroral oval, or indirectly from the cusp or polar cap. In the latter case, O+ ions fly along the open field lines and enter the plasma sheet due to the global scale plasma convection. A key difference between the two mechanisms is the timescale. O+ outflows from nightside auroral oval can reach the plasmapause in several minutes (Gkioulidou et al., 2019; Nosé et al., 2022), whereas the timescale for those from the cusp or polar cap is 10s of minutes or even several hours (Chappell et al., 2008). Based on the test particle tracing, we show that the energy-time dispersions of H+ and O+ in the parallel and anti-parallel directions are consistent with a common energization source for both ion species. The outflow source region was located around 1.2 R_E above the nightside auroral region in both hemispheres.

The outflow source location is consistent with the typical altitude of AAR (1–3 R_E altitude) (Karlsson et al., 2020; Paschmann et al., 2003). In addition, the fact that the highest energy for H+ and O+ outflows is both ∼1 keV suggests that the outflows are energized through a quasi-static potential drop. In contrast, perpendicular heating would lead to an energization dependent on the ion mass (Chang et al., 1986). Note that in the test particle tracing, we have assumed that the outflows are conics, which seems to be inconsistent with the parallel acceleration through a potential drop. However, if we were to launch the test particles at the altitude of 1.2 R_E by assuming a beam distribution along the magnetic field, the simulation results would be quantitatively similar to those shown in Figure 6. Therefore the simulation results are compatible with both parallel acceleration and perpendicular heating. However, the peak energies of both H+ and O+ are the same instead of mass independent, favoring the parallel acceleration.

The number flux of the O+ outflows from the nightside auroral region is on the order of $10^8 - 10^9$ #/cm^2-s in this event (normalized to 100 km altitude). As a comparison, previous studies documented that during the main phase of the 25 September 1998 storm, which had a similar minimum Dst as the 17 March 2015 storm, the ion outflows from the cusp were $10^9 - 10^{10}$ #/cm^2-s (Moore, Peterson, et al., 1999; Strangeway et al., 2005) and those from the auroral region were, when normalized to 100 km altitude, $10^8 - 10^9$ #/cm^2-s (Zhao et al., 2022). The latter is comparable to what was observed in this event (Figure 8d). The O+ outflows from the nightside auroral region are likely to be one order of magnitude smaller than those from the cusp. However, in the former case, essentially all ion outflows can enter the plasma sheet in several minutes, whereas in the latter case, ions would be convected to the nightside, causing a time delay on the order of several 10s min and could be significantly lost through the open field lines. Therefore, we suggest that the dominant source for the newly formed plasma cloak is the ion outflows from the nightside auroral region. On the other hand, the cusp and polar cap outflows could still be an important

source for sustaining the already-formed plasma cloak, because they are dominant in number flux, take longer to reach the inner magnetosphere, and could be heated through betatron acceleration.

To further discuss the physical processes in the inner magnetosphere, we return to Figures 3 and 4, which show the first RBSP-B and -A orbits during the storm's main phase. Comparing the outbound and inbound passes for both spacecraft, we note that the inbound passes saw much more 100s eV plasma cloak ions and also keV plasma sheet ions (Panels d and e). The missing plasma cloak and plasma sheet ions are probably because of the shadowing due to the strong magnetopause erosion (Le et al., 2016). Their re-appearance in the inbound passes suggests that the ionosphere-magnetosphere system had actively responded to refill these ions.

Within the first orbit of RBSP-A (Figure 4, we observed a transition from the outflows to mirroring outflows, and then to bi-directional plasma cloaks. Before 12 UT, many O+ outflows were observed (Panels e and f). In this particular event, outflows are around 0 deg pitch angle because both spacecraft were in the southern hemisphere (Panel j). No significant mirrored population or outflow from the farther hemisphere was observed, possibly because the magnetic field lines were tail-like and dynamic beyond L∼4 (Panel a). The strong stretching leads to scattering by the cross-tail current when ions pass the magnetic equator. The stretching may also lead to a longer travel time, causing these ions to convect to a lower L value and miss the spacecraft. As the spacecraft moved toward the perigee (12 UT to 13:30 UT), we start to see mirroring outflows from both hemispheres, probably because the field lines were less dynamic and more dipole at lower L values. A detailed analysis is presented in Figure 6 and Section 3.4 for the KAWs #8 in Figure 4. After 13:30 UT, the mirroring outflows smoothly transited into the bi-directional plasma cloak. The smooth transition is also a good indicator that the former is an immediate source, in terms of energy and location, for the plasma cloak. As shown in Figure 8 and Section 3.5, the auroral outflows have enough flux to account for the newly formed plasma cloak.

Note that our discussion is primarily for O+ ions. This is because O+ ions are of ionospheric origin, whereas H+ ions can be from the ionosphere or the plasma sheet. However, as we showed in Figure 6, when H+ outflows are strong, their dispersions can exceed the background plasma sheet H+ ions. Therefore, what we have proposed for O+ ions/plasma cloak should work the same for H+ ions/plasma cloak. For example, in Figures 3 and 4, both RBSP-A and -B did not see much H+ plasma cloak (10–100s eV) in the outbound passes (Panel d). In the inbound passes, a newly formed H+ plasma cloak was observed.

In contrast to the low-energy ions proposed by Chappell et al. (2008), the auroral ions are different in the following aspects. First, the auroral ions are energy ready. They are already 10–100s eV, whereas low-energy ions (several eV) need to go through centrifugal acceleration. Second, the auroral ions need only several minutes to form the plasma cloak. This travel time is much shorter than that for low-energy ions (several hours) because the auroral field lines map directly to outside the plasmapause and the auroral ions are high-energy (and thus high parallel velocity). However, it is important to note that the auroral ions are probably an additional source for the plasma cloak. In other words, our proposed mechanism complements, instead of ruling out, the Chappell et al. (2008) mechanisms. The auroral ions are likely to provide an initial population for the plasma cloak, whereas the low-energy ions provide a sustaining population in the later hours (cf. Figure 10).

5. Conclusions

We investigated the geomagnetic storm on 17 March 2015, focusing on the coupled system between the nightside auroral oval and the plasma sheet within the inner magnetosphere. We observed that the motion of the equatorward boundary of the auroral oval (Figure 2) is consistent with the inward motion of the inner boundary of the plasma sheet (Figure 3), which is also consistent with the inward motion of the plasmapause (Figure 1). Based on these observations, we summarize our main conclusions in Figure 10 and list them below:

1. Correlated KAWs and O+ outflows were observed repetitively within the plasma sheet by both RBSP-A and -B (Figures 3 and 4). Test particle tracing shows that the O+ outflows originate from the nightside auroral oval (Figure 6). The energy budget shows that the Poynting flux associated with KAWs is adequate to power the observed auroral emission and the kinetic energy of the O+ outflows (Figure 8). Therefore, we suggest KAWs are the main driver for the O+ outflows and the auroral emission.
2. The plasma cloak emerged after intense O+ outflows (Figures 8 and 9). The number flux of the O+ outflow is adequate to explain the formation of the plasma cloak (Figure 8), suggesting that the O+ outflows from the nightside auroral oval could be a dominant source of the initial formation of the plasma cloak. The O+

outflows from the cusp and polar cap may be important in sustaining the newly formed plasma cloak in later hours.

Data Availability Statement

The THEMIS ASI data are available at https://cdaweb.gsfc.nasa.gov/pub/data/themis/thg. The RBSP data (HOPE, EFW, and EMFISIS) are available at https://cdaweb.gsfc.nasa.gov/pub/data/rbsp. The DMSP SSUSI data are available at https://cdaweb.gsfc.nasa.gov/pub/data/dmsp/. The other DMSP data used in this study are available at http://cedar.openmadrigal.org/.

Acknowledgments
ST acknowledge NASA Grants 80NSSC19K0306 and 80NSSC22K1027. QM would like to acknowledge the NASA Grants 80NSSC20K0196 and 80NSSC24K0572, and NSF Grant AGS-2225445. JL and JB acknowledge NASA Grants LWS- 80NSSC20K0201, 80NSSC21K0522, 80NSSC18K1227, and NNX14AI18G, and the Grant DE-SC0010578.

References

André, M., & Yau, A. W. (1997). Theories and observations of ion energization and outflow in the high latitude magnetosphere. *Space Science Reviews*, *80*(1/2), 27–48. https://doi.org/10.1023/A:1004921619885

Breneman, A. W., Wygant, J. R., Tian, S., Cattell, C. A., Thaller, S. A., Goetz, K., et al. (2022). The van Allen probes electric field and waves instrument: Science results, measurements, and access to data. *Space Science Reviews*, *218*(8), 69. https://doi.org/10.1007/s11214-022-00934-y

Chang, T., Crew, G. B., Hershkowitz, N., Jasperse, J. R., Retterer, J. M., & Winningham, J. D. (1986). Transverse acceleration of oxygen ions by electromagnetic ion cyclotron resonance with broad band left-hand polarized waves. *Geophysical Research Letters*, *13*(7), 636–639. https://doi.org/10.1029/GL013i007p00636

Chappell, C. R., Huddleston, M. M., Moore, T. E., Giles, B. L., & Delcourt, D. C. (2008). Observations of the warm plasma cloak and an explanation of its formation in the magnetosphere. *Journal of Geophysical Research*, *113*(A9), A09206. https://doi.org/10.1029/2007JA012945

Chaston, C. C., Bonnell, J. W., Kletzing, C. A., Hospodarsky, G. B., Wygant, J. R., & Smith, C. W. (2015). Broadband low-frequency electromagnetic waves in the inner magnetosphere. *Journal of Geophysical Research: Space Physics*, *120*(10), 8603–8615. https://doi.org/10.1002/2015JA021690

Cladis, J. B. (1986). Parallel acceleration and transport of ions from polar ionosphere to plasma sheet. *Geophysical Research Letters*, *13*(9), 893–896. https://doi.org/10.1029/GL013i009p00893

Funsten, H. O., Skoug, R. M., Guthrie, A. A., MacDonald, E. A., Baldonado, J. R., Harper, R. W., et al. (2013). Helium, oxygen, proton, and electron (HOPE) mass spectrometer for the radiation belt storm probes mission. *Space Science Reviews*, *179*(1–4), 1–62. https://doi.org/10.1007/s11214-013-9968-7

Gkioulidou, M., Ohtani, S., Ukhorskiy, A. Y., Mitchell, D. G., Takahashi, K., Spence, H. E., et al. (2019). Low-energy (<kev) O+ ion outflow directly into the inner magnetosphere: Van Allen probes observations. *Journal of Geophysical Research: Space Physics*, *124*, 405–419. https://doi.org/10.1029/2018JA025862

Hardy, D. A. (1984). *Precipitating electron and ion detectors (SSJ/4) for the block 5D/flights 6-10 DMSP satellites: Calibration and data presentation*. Space Physics Division, Air Force Geophysics Laboratory.

Horwitz, J. L., Ho, C. W., Scarbro, H. D., Wilson, G. R., & Moore, T. E. (1994). Centrifugal acceleration of the polar wind. *Journal of Geophysical Research*, *99*(A8), 15051–15064. https://doi.org/10.1029/94ja00924

Hull, A. J., Chaston, C. C., Bonnell, J. W., Wygant, J. R., Kletzing, C. A., Reeves, G. D., & Gerrard, A. (2019). Dispersive Alfvén wave control of O^+ ion outflow and energy densities in the inner magnetosphere. *Geophysical Research Letters*, *46*(15), 8597–8606. https://doi.org/10.1029/2019GL083808

Karlsson, T., Andersson, L., Gillies, D. M., Lynch, K., Marghitu, O., Partamies, N., et al. (2020). Quiet, discrete auroral arcs—Observations. *Space Science Reviews*, *216*(1), 1–50. https://doi.org/10.1007/S11214-020-0641-7

Keiling, A., Parks, G. K., Rème, H., Dandouras, I., Wilber, M., Kistler, L., et al. (2006). Energy-dispersed ions in the plasma sheet boundary layer and associated phenomena: Ion heating, electron acceleration, Alfvén waves, broadband waves, perpendicular electric field spikes, and auroral emissions. *Annales Geophysicae*, *24*(10), 2685–2707. https://doi.org/10.5194/ANGEO-24-2685-2006

Keiling, A., Rème, H., Dandouras, I., Bosqued, J. M., Parks, G. K., McCarthy, M., et al. (2004). Transient ion beamlet injections into spatially separated PSBL flux tubes observed by cluster-cis. *Geophysical Research Letters*, *31*(12), L12804. https://doi.org/10.1029/2004GL020192

Keiling, A., Wygant, J. R., Cattell, C. A., Mozer, F. S., & Russell, C. T. (2003). The global morphology of wave poynting flux: Powering the aurora. *Science*, *299*(5605), 383–386. https://doi.org/10.1126/science.1080073

Kletzing, C. A., Kurth, W. S., Acuna, M., MacDowall, R. J., Torbert, R. B., Averkamp, T., et al. (2013). The electric and magnetic field instrument suite and integrated science (EMFISIS) on RBSP. *Space Science Reviews*, *179*(1–4), 127–181. https://doi.org/10.1007/s11214-013-9993-6

Kolmogorov, A. N. (1941). In *Dissipation of energy in locally isotropic turbulence* (Vol. 32, pp. 16–18).

Le, G., Lühr, H., Anderson, B. J., Strangeway, R. J., Russell, C. T., Singer, H., et al. (2016). Magnetopause erosion during the 17 March 2015 magnetic storm: Combined field-aligned currents, auroral oval, and magnetopause observations. *Geophysical Research Letters*, *43*(6), 2396–2404. https://doi.org/10.1002/2016GL068257

Liu, Z. Y., & Zong, Q. G. (2022). Ionospheric oxygen outflows directly injected into the inner magnetosphere: Van Allen probes statistics. *Journal of Geophysical Research: Space Physics*, *127*, e2022JA030611. https://doi.org/10.1029/2022JA030611

Lysak, R. L. (2023). Kinetic Alfvén waves and auroral particle acceleration: A review. *Reviews of Modern Plasma Physics*, *7*(1), 1–28. https://doi.org/10.1007/S41614-022-00111-2

Lysak, R. L., & Lotko, W. (1996). On the kinetic dispersion relation for shear Alfvén waves. *Journal of Geophysical Research*, *101*(A3), 5085–5094. https://doi.org/10.1029/95JA03712

Mende, S. B., Harris, S. E., Frey, H. U., Angelopoulos, V., Russell, C. T., Donovan, E., et al. (2008). The THEMIS array of ground-based observatories for the study of auroral substorms. *Space Science Reviews*, *141*(1–4), 357–387. https://doi.org/10.1007/s11214-008-9380-x

Moore, T. E., Lundin, R., Alcaydé, D., André, M., Ganguli, S. B., Temerin, M., & Yau, A. W. (1999). Source processes in the high-latitude ionosphere. *Space Science Reviews*, *88*(1/2), 7–84. https://doi.org/10.1023/A:1005299616446

Moore, T. E., Peterson, W. K., Russell, C. T., Chandler, M. O., Collier, M. R., Collin, H. L., et al. (1999). Ionospheric mass ejection in response to a CME. *Geophysical Research Letters*, *26*(15), 2339–2342. https://doi.org/10.1029/1999GL900456

Nosé, M., Keika, K., Kletzing, C. A., Spence, H. E., Smith, C. W., MacDowall, R. J., et al. (2016). Van Allen probes observations of magnetic field dipolarization and its associated O+ flux variations in the inner magnetosphere at L < 6.6. *Journal of Geophysical Research: Space Physics*, *121*(8), 7572–7589. https://doi.org/10.1002/2016JA022549

Nosé, M., Matsuoka, A., Miyoshi, Y., Asamura, K., Hori, T., Teramoto, M., et al. (2022). Flux enhancements of field-aligned low-energy O^+ ion (FALEO) in the inner magnetosphere: A possible source of warm plasma cloak and oxygen torus. *Journal of Geophysical Research: Space Physics*, *127*. https://doi.org/10.1029/2021JA030008

Paschmann, G., Håland, S., & Treumann, R. (2003). *Auroral plasma physics*. Kluwer Academic Pub. Retrieved from http://books.google.com/books?id=xYFjIrDlGqIC

Paxton, L. J., Morrison, D., Zhang, Y., Kil, H., Wolven, B., Ogorzalek, B. S., & Meng, C.-I. (2002). *Validation of remote sensing products produced by the special sensor ultraviolet scanning imager (SSUSI): A far UV-imaging spectrograph on DMSP f-16*. In A. M. Larar & M. G. Mlynczak (Eds.), (Vol. 4485, p. 338–348). SPIE. https://doi.org/10.1117/12.454268

Ripoll, J. F., Thaller, S. A., Hartley, D. P., Cunningham, G. S., Pierrard, V., Kurth, W. S., et al. (2022). Statistics and empirical models of the plasmasphere boundaries from the van Allen probes for radiation belt physics. *Geophysical Research Letters*, *49*(21), e2022GL101402. https://doi.org/10.1029/2022GL101402

Stern, D. P. (1975). The motion of a proton in the equatorial magnetosphere. *Journal of Geophysical Research*, *80*(4), 595–599. https://doi.org/10.1029/ja080i004p00595

Strangeway, R. J., Ergun, R. E., Su, Y.-J., Carlson, C. W., & Elphic, R. C. (2005). Factors controlling ionospheric outflows as observed at intermediate altitudes. *Journal of Geophysical Research*, *110*(A3), A03221. https://doi.org/10.1029/2004JA010829

Thaller, S. A., Wygant, J. R., Cattell, C. A., Breneman, A. W., Tyler, E., Tian, S., et al. (2019). Solar rotation period driven modulations of plasmaspheric density and convective electric field in the inner magnetosphere. *Journal of Geophysical Research: Space Physics*, *124*, 1726–1737. https://doi.org/10.1029/2018JA026365

Tian, S., Colpitts, C. A., Wygant, J. R., Cattell, C. A., Ferradas, C. P., Igl, A. B., et al. (2021). Evidence of Alfvenic poynting flux as the primary driver of auroral motion during a geomagnetic substorm. *Journal of Geophysical Research: Space Physics*, *126*(5), e2020JA029019. https://doi.org/10.1029/2020JA029019

Tian, S., Lyons, L. R., Nishimura, Y., Wygant, J. R., Lysak, R. L., Ferradas, C. P., et al. (2022). Auroral beads in conjunction with kinetic Alfvén waves in the equatorial inner-magnetosphere. *Geophysical Research Letters*, *49*(9), e2022GL098457. https://doi.org/10.1029/2022GL098457

Tsyganenko, N. A. (1989). A magnetospheric magnetic field model with a warped tail current sheet. *Planetary and Space Science*, *37*(1), 5–20. https://doi.org/10.1016/0032-0633(89)90066-4

Volland, H. (1973). A semiempirical model of large-scale magnetospheric electric fields. *Journal of Geophysical Research*, *78*(1), 171–180. https://doi.org/10.1029/JA078i001p00171

Wang, C.-P., Wang, X., Lin, Y., Wing, S., & Hairston, M. (2023). Energy-dispersive field-aligned warm ion enhancement in the plasma sheet during a substorm growth phase: A THEMIS event. *Journal of Geophysical Research: Space Physics*, *128*(5), e2022JA031252. https://doi.org/10.1029/2022JA031252

Wygant, J. R., Bonnell, J. W., Goetz, K., Ergun, R. E., Mozer, F. S., Bale, S. D., et al. (2013). The electric field and waves instruments on the radiation belt storm probes mission. *Space Science Reviews*, *179*(1–4), 183–220. https://doi.org/10.1007/s11214-013-0013-7

Wygant, J. R., Keiling, A., Cattell, C. A., Johnson, M., Lysak, R. L., Temerin, M., et al. (2000). Polar spacecraft based comparisons of intense electric fields and poynting flux near and within the plasma sheet-tail lobe boundary to UVI images: An energy source for the aurora. *Journal of Geophysical Research*, *105*(A8), 18675–18692. https://doi.org/10.1029/1999JA900500

Wygant, J. R., Keiling, A., Cattell, C. A., Lysak, R. L., Temerin, M., Mozer, F. S., et al. (2002). Evidence for kinetic Alfvén waves and parallel electron energization at 4-6 re altitudes in the plasma sheet boundary layer. *Journal of Geophysical Research*, *107*(A8), 1201. https://doi.org/10.1029/2001JA900113

Yau, A. W., & André, M. (1997). Sources of ion outflow in the high latitude ionosphere. *Space Science Reviews*, *80*(1/2), 1–25. https://doi.org/10.1023/A:1004947203046

Yue, C., Wang, C.-P., Nishimura, Y., Murphy, K. R., Xing, X., Lyons, L., et al. (2015). Empirical modeling of 3-D force-balanced plasma and magnetic field structures during substorm growth phase. *Journal of Geophysical Research: Space Physics*, *120*(8), 6496–6513. https://doi.org/10.1002/2015JA021226

Zhao, K., Kistler, L. M., Lund, E. J., Nowrouzi, N., Kitamura, N., & Strangeway, R. J. (2022). Nightside auroral H+ and O+ outflows versus energy inputs during a geomagnetic storm. *Journal of Geophysical Research: Space Physics*, *127*(11), e2022JA030923. https://doi.org/10.1029/2022JA030923